Journal of Manufacturing Processes 84 (2022) 660–668

Contents lists available at ScienceDirect

Journal of Manufacturing Processes

journal homepage: www.elsevier.com/locate/manpro

Technical paper

Parametric design optimisation of tree-like support structure for the laser-based powder bed fusion of metals

Sebastian Weber [a,b,*], Joaquin Montero [a,b], Matthias Bleckmann [b], Kristin Paetzold [c]

[a] Universität der Bundeswehr München, Institute for Technical Product Development, 85579 Neubiberg, Germany
[b] Bundeswehr Research Institute for Materials, Fuels and Lubricants (WIWeB), 85435 Erding, Germany
[c] Technische Universität Dresden, Institute of Machine Elements and Machine Design, 01069 Dresden, Germany

ARTICLE INFO

Keywords:
Additive manufacturing
Laser powder bed fusion
Support structure
Parameter optimisation
Design for additive manufacturing

ABSTRACT

Support structure design for Laser Powder Bed Fusion has received little attention in Design for Additive Manufacturing although its importance for a successful and efficient build job. The resulting knowledge insufficiency on support design can lead to in-process failures of the build. Also, parts can crack due to high, unaccounted residual stresses. This, and overestimated support designs, lead to an increased manufacturing time and cost. The presented research contributes to a better understanding of support structure design by developing a workflow for the design of tree-like support structure and its subsequent meta-model based parameter optimisation. The design parameters of resulting support structures for two generic geometries in a cantilever shape with a planar and an arched down-facing surface are compared with each other, showing consistent values for the minimum distance between branches and the branch length. These and other design parameters govern the geometry of the tree-like structure within the design space. An additionally performed sensitivity study revealed high correlations of the stem diameter with the part's displacements. Based on 500 individual support designs and the meta-model evaluation of 9000 parameter sets, a Pareto frontier emerges for the trade-off between the minimum support structure volume and the part's displacements.

1. Introduction

In the laser-based powder bed fusion of metals (PBF-LB/M), an additive manufacturing (AM) process, support structures are needed to support overhanging surfaces or anchor the part to the base plate [1]. Over the last few years, many Design for AM (DfAM) guidelines and rules of thumb were established [2,3]. These DfAM guidelines usually deal only with the part design and how to avoid support structures rather than their design. In addition, many investigations apply topology optimisation with additional constraints regarding the overhang angle [4,5] for enhanced printability as a restrictive approach on the part design. Recently constraints are also added for residual stresses to prevent build failure [6]. Only a few studies focus on an opportunistic design of supports [7,8]. This leads to a lack of knowledge and insufficient understanding of support structure design, which is expressed by the little number of investigations on overhanging structures and the therefrom resulting residual stress formation [9]. The paper at hand aims to contribute to a better understanding of support structure design by using a parameter optimisation of a parametric tree-like support structure as an example. To keep the focus on the support design and limit the number of variables in the optimisation, process variables are kept constant during the simulations and considered to be given by the machine's manufacturer. One of the most critical issues in metal AM is the build failure or deformations, due to residual stress in the part [10], which may happen during or after the process has finished. To reduce the risk of in-process failure, some investigations were made on optimising support structures for reduced residual stresses or less part deformation. These investigations commonly involve topology optimisation for support structure design or to create a density map, which can further be used for an easy support generation using lattice structures or unit cells [10,11]. Topology optimised support structure has the disadvantage that its faceted geometry usually needs some kind of smoothing and cannot be further processed in CAD tools without adaption [12]. The optimisation of the parametric tree-like support presented in this paper on the other hand uses CAD compatible non-uniform rational basis splines (NURBS). Another benefit of parameter optimisation is the fast processing, once the meta-model exists. This way, possible support designs for recurring generalised support surfaces can be determined and support structure parameters can be set specifically for such geometries without the need for computationally expensive topology optimisation.

* Corresponding author at: Universität der Bundeswehr München, Institute for Technical Product Development, 85579 Neubiberg, Germany.
E-mail address: s.weber@unibw.de (S. Weber).

https://doi.org/10.1016/j.jmapro.2022.09.063
Received 16 July 2021; Received in revised form 17 August 2022; Accepted 29 September 2022
Available online 26 October 2022
1526-6125/© 2022 The Author(s). Published by Elsevier Ltd on behalf of The Society of Manufacturing Engineers. This is an open access article under the CC BY-NC-ND license (http://creativecommons.org/licenses/by-nc-nd/4.0/).

Several studies exist for the topology, but not the parameter optimisation of support structure. Studies involving topology optimisation can be classified by their approach regarding the mechanical behaviour, the thermal behaviour, or coupled investigations. A few publications, which use tree-like or similar support structures, are mentioned hereafter. The mechanical compliance is for example the objective in the investigations of Mezzadri et al. [13], Zhang et al. [14], and Liu et al. [15]. Their studies use or result in tree-like support structure. This support type is also part of the investigations of Malekipour et al. [16], Zhou et al. [17] and Miki and Nishiwaki [18], which tackle the objective of increasing heat conduction. Tree-like supports are considered an effective support solution, especially when optimised for a minimal thermal compliance [19]. Combined mechanical and thermal loads are considered for tree-like support by Allaire and Bogosel [20] and Giraldo-Londoño et al. [21]. Despite the large number of investigations using topology optimisation, Zhang et al. [22] created a parametric support structure, which was optimised for reduced support volume. In contrast to their and other existing approaches, design parameters, residual stresses, and thermal warping were considered in the parameter optimisation of the here presented approach. This once more highlights the novelty of this study. Section 2 starts with a detailed description of automatic support generation using parametric tree-like structures, followed by the set-up of a sequential thermal and structural simulation model. A subsequent parameter optimisation based on a meta-model for two generic geometries is described afterwards. Results of this parameter optimisation are presented and discussed in Section 3 together with a verification of the supports' functionality by a comparison with commercially generated block-support. The study concludes with a short summary and suggestions for future research.

2. Methodology

This section describes the approach for an automated generation of biomimetic tree-support and its subsequent adaption through parameter optimisation. For this, an additive manufacturing process simulation is carried out to evaluate the total displacements of a generic part after cool down, using the tree-support. The parameter optimisation is based on a set of design points (DP), where each DP is a set of parameters leading to a specific geometry of the support structure. These design points are created and evaluated iteratively until a specified prediction accuracy is met. In this way, the necessary amount of calculations can be kept to a minimum. Additionally, a sensitivity study is performed to figure out correlations between parameters and to estimate the effect of each parameter on the results. Two different generic geometries are chosen for the automated tree-support generation. The resulting parameter optimised tree structures are compared against each other in Section 3.

2.1. Automated parametric support generation

Common bio-inspired approaches for realistic tree representations in computer graphics rely on recursive algorithms such as the Lindenmayer system (L-system) [23–25]. For the complex case of PBF-LB/M, tree-like supports using the L-system turned out to be impractical. Reasons for this are the bottom-up approach, i.e. the trees grow from the stem, the high order of branching or the complexity to parameterise the system. Additionally, more organic structures can be created using the new method introduced in this section, since the guiding splines have at least a G1 continuity. The support geometry is generated within the commercial software ANSYS® SpaceClaim® using the Python® programming language.

2.1.1. Design parameters

The design parameters used for creating the tree-support can be classified into two groups. The first set of parameters defines the geometry directly and is therefore used for optimisation. The second set contains parameters, which control some boundary conditions of the support generation and are therefore kept constant during parameter optimisation. Dimensional parameters, except the reduction factor k_{red}, belonging to the first group are explained in Fig. 1. The reduction factor k_{red} describes the relationship between points on the support surface and the number of points for the stems. Points on the support surface are further called seed points, as they build the grid that defines the tree generation. Dimensional parameters are the diameter for the top part of the structure d_{top}, the stem diameter d_{stem}, the minimum distance between branches l_{min} as well as parameters for the continuity representation l_{stem} and l_{top}, see Fig. 1. The latter set the length for a straight line extending from the support surface or respectively the base surface. Parameters of the second group are used to control the behaviour. The representation accuracy can be set as well as a binary value expressing a perpendicular or non-perpendicular attachment of the branches to the support faces. One additional parameter is the surface angle – measured in respect to the horizontal – below which the surfaces require support. Distinct values for parameters of the first group can vary in a specified range, which is listed and further discussed in Table 1 of Section 2.3.

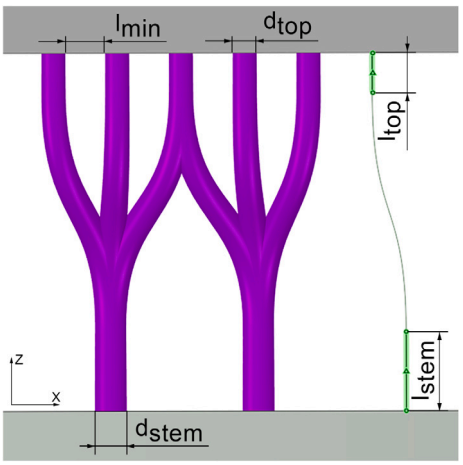

Fig. 1. Tree-support design parameters shown on the generated support geometry and the guiding skeleton.

2.1.2. Determination of overhanging surfaces

After the parameters are initialised in the Python® script, the surfaces requiring support need to be determined. For this, all surfaces of the build body with a z-coordinate of the face midpoint larger than the one from the base surface are checked for their face normal direction. To determine all possible candidate surfaces that might need support, the z-component of the normal vector is checked for a negative value. The need for support is later checked for each seed point of the support branches individually using the surface angle parameter and the angle of the face normal evaluated at the seed point. For the PBF-LB/M process the surface angle parameter is set to 45° as this is known in literature as the critical angle for self-supporting surfaces [26,27]. Another method to determine the points on the part needing support is presented by Wang et al. [28].

2.1.3. Seed points and number of stems

The third step in the support generation is the calculation of necessary seed points. For this, the support surfaces are assumed to have a rectangular outline with the lengths l_X and l_Y respectively along the x- and y-coordinate system. The number of seed points in x- and y-direction can be calculated by rounding the result of Eq. (1) to full integer values.

$$n_{seedsX} = \frac{l_X}{(d_{top} + l_{min})}; \quad n_{seedsY} = \frac{l_Y}{(d_{top} + l_{min})} \tag{1}$$

The number of stems n_{stems} is then determined by multiplying the number of seeds with the reduction factor k_{red}. The resulting value is floored and converted to an integer data type. In order to determine the exact position of each seed on the support surface, the edge distance x_{edge} is calculated by the following Eq. (2) and a pitch value representing the distance between the seed points needs to be known.

$$x_{edge} = \frac{\left[l_X - \left[n_{seedsX} \cdot d_{seed} + \left(n_{seedsX} - 1\right) \cdot l_{min}\right]\right]}{2} \tag{2}$$

The normal angle of the surface is evaluated at each seed point. Seed points are only further evaluated if the resulting angle is smaller than the critical angle. This procedure is followed by the determination of possible stems for each support surface. The location of the stems is figured out on the support surface and then projected onto the base surface. After this, a second set for stem and seed points is created. A copy of the stem points is moved along the global z-axis by the amount specified in l_{stem}. For the seed points, this step is followed respectively along the negative z-axis with l_{top} or along the support face normal, if the corresponding binary value is set to one.

2.1.4. Creation of the branches

The distance to the stem points is calculated for each of the previously determined seed points individually. Each branch is then created one after another for every seed point and the matching stem points with the shortest distance within a small tolerance. For this, a function takes a point list with four points – the seed point, the stem point as well as the two points for continuity – and the face normal as arguments. Next, the start and end line are created followed by a spline connecting them. At the seed and the stem point the circular cross-sections are then created perpendicular to the given face normal or the global z-direction with the corresponding diameters d_{top} or d_{stem} respectively. Finally, a transition loft is created by sweeping one cross-section to the other along the three guiding curves.

The last steps of the script are the combining of the single branches to complete trees using Boolean functions and the creation of so-called named selections. These selection sets can later be used in the ANSYS® Mechanical™ application. The sets include various selections of faces for boundary conditions as well as the support structure, base and build body itself.

2.2. Additive manufacturing process simulation

The simulation model of the complete manufacturing process is created using the commercial simulation software ANSYS® Workbench™ in the version 2020 R2, following the software's approach for the simulation of the additive manufacturing process. The additive process is implemented as an uncoupled simulation with a thermal simulation followed by a structural simulation that uses the strain results of the thermal simulation as an input. During the simulation, complete layers of elements are consecutively activated at the melting temperature of the material. In this way, the computational expensive simulation of the laser scanning path can be avoided. A build and cool-down phase is simulated, leading to the thermal history of the part. These element layers are the so-called super layers, consisting of multiple physical layers [29].

2.2.1. Geometry and material

The geometry for the simulation model is split into three parts. The base plate, the build body and the support geometry. The base plate is a circular plate with a diameter of 100 mm and a thickness of 25 mm. As described in Section 2.1, the support geometry is created automatically for parameters specified in Section 2.3 and changes therefore for each parameter set that is simulated. To investigate not only the support scenario for flat overhanging surfaces but also for more round and complex surfaces, two different build geometries were simulated. The first part is a standard cantilever that is used by ANSYS® for the calculation of the strain scaling factor, which is further referred to as *Cantilever A*. It is displayed in Fig. 2(a). The geometry in form of a cantilever was chosen because of the large overhang. Additionally, it is frequently used in research on support optimisation in some variations [10,11,30] and allows thereby for result comparisons. The dimensions, which are shown in the Figure, were taken from the ANSYS® example for the same reason of comparability. The second build geometry, which is referred to as *Cantilever B*, is also modelled in the shape of a cantilever and therefore shares the length, width and minimal support height of the first body. The difference is the arched surface that needs support. The overall height of the cantilever increases to 14 mm to compensate for the changing thickness of the top section. The second build body is shown with some dimensions in Fig. 2(b).

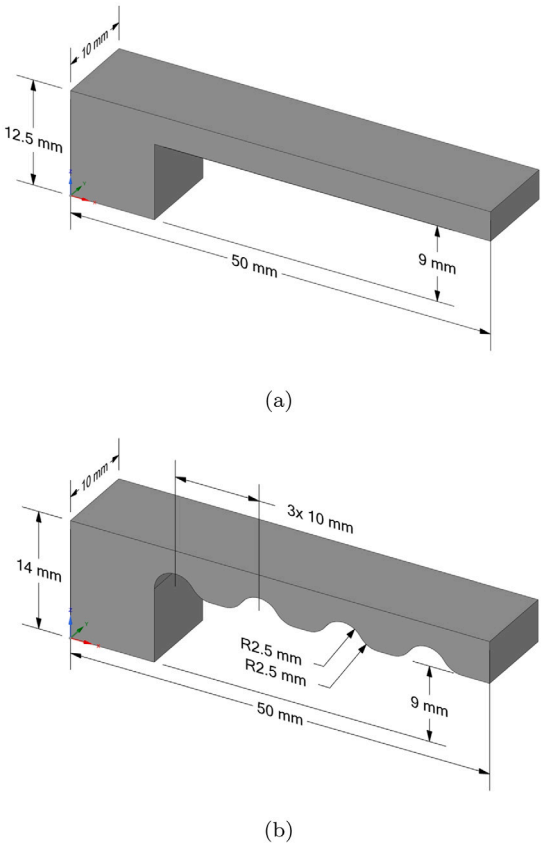

Fig. 2. Cantilever geometry used for the simulation models with a flat overhang for Cantilever A in (a) and an arched down-facing surface for Cantilever B in (b).

All parts of the simulation model use the titanium alloy Ti6Al4V of the ANSYS® standard material library for additive manufacturing materials with temperature-dependent properties for density, specific heat, thermal conductivity and tensile properties. The material uses isotropic elasticity and bi-linear isotropic hardening for the representation of plastic deformations. Previous investigations showed a by around 10% reduced tensile strength for additively manufactured support structures with small diameters, because of additional powder particles that conglomerate to the outside boundaries [31], which is considered in the model for this study by multiplying the material properties for the support structure with a support property factor of 0.9. For a correct simulation of the thermal strains, the reference temperature at which no strains occur needs to be set. For the base plate, this equals the ambient temperature. For the build body and support structure, on the other hand, the reference temperature is the melting temperature of the used material — in this case 1605 °C.

2.2.2. Meshing and contacts

In a previously published article, two different meshing strategies for additive manufacturing simulation were compared. For geometries with a high level of curvature, such as tree-like support structure, layered tetrahedral meshing turned out to be more practical [32]. The tetrahedral shape of the elements allows for a better representation of the geometry compared to a cartesian or voxel mesh, even with a larger element size. This results in shorter simulation times with the same or better result accuracy, which is especially beneficial for a large number of necessary simulations in the parameter study presented in this article. For this simulation, the layered tetrahedral mesh is used with a quadratic element behaviour and a layer height for the tetrahedral layers of 0.5 mm, which is in accordance with the element size of 0.5 mm for the part. The support structure and the contact region between the support and the part is meshed with an element size of 0.25 mm for a better representation of the small diameter of the stems and branches as well as a better convergence of the solver at the contact pair. To avoid issues during the solution process, the element size is selected carefully to match an integer multiple of the layer height resulting in two elements in height per layer. The size for the elements of the base body is set to 5 mm, as they have only a small influence on the overall simulation results. The model has three contact regions. The contact between the base plate and the build part as well as between the base and the support structure is a fully bonded contacts with default settings. The more challenging contact between the support structure and the build geometry uses also a fully bonded contact, but with reduced contact stiffness. A reduction factor of 0.1 for the stiffness leads to a better convergence of the solver. Additionally, the method for contact detection is set to node-normal to target, which translates to support structure towards the build part.

2.2.3. AM-process settings and boundary conditions

The value for the simulation layer height needs to be the same or an integer multiple of the mesh layer height. For these simulations, the layer height is set to 0.5 mm for faster calculations and exceeds thereby the recommended range of 10–20 times of the physical layer height [29], which is 20 (mμ) for the selected Trumpf TruPrint 1000 PBF-LB/M machine. The deviations using a larger layer height of 25 times the physical layer height is negligible as shown in a previous study [32]. Other process parameters include the hatch distance with 80 (mμ) and the scanning speed of 905 mm s^{-1}. The simulation uses a single heat source and the time between layers is set to 10 s. The simulation model was validated by a previous set of experiments and simulations, from which a strain scaling factor of 0.1663 was derived. This scaling factor allows achieving more accurate and realistic results for the used PBF-LB/M system.

For the boundary conditions of the model, the ambient temperature during the build process is set to 40 °C and during cool-down to 24 °C. Thereby the gas convection coefficient for the combination of Argon and the Titanium alloy Ti6Al4V is approximated with 6 W m^{-2} K^{-1}, following the range reported by Li et al. [33] The approximation is done using laws for ideal gases, empirical data and equations given by the Association of German Engineers (VDI) [34]. As the powder is not simulated, the heat transfer between the powder and the part is implemented using a convective coefficient, which is assumed to be 1% of the gas convection coefficient. Additional thermal boundary conditions are applied to the lower surface of the base plate. During the build process, the heat transfer at this surface is neglected and therefore implemented as an adiabatic condition, following the work of Romano et al. [35] For the cool-down step, a constant ambient temperature of 24 °C is assumed. On the structural side, also the bottom surface of the base plate is used to apply boundary conditions. All elements of this surface are fixed in the x-, y- and z-coordinate.

The additive manufacturing process simulation is divided into a thermal and a structural simulation. Each simulation is further divided into two steps, one for the heating and one for the cool-down phase. These two steps are repeated for each simulation layer. After the cool-down step of the finished build process in the structural simulation back to ambient temperature, one additional step for the removal of the support structure is added. The large deformation option of the structural simulation is used to account for non-linear behaviour and to allow plastic deformations of the parts.

Table 1
Parameter ranges used for the design point creation.

	d_{stem}	d_{top}	l_{stem}	l_{top}	l_{min}	k_{red}
min [mm]	0.5	0.5	0.5	0.5	0.5	−0.5 [–]
max [mm]	0.8	0.8	2.5	2.5	1.5	0.6 [–]

2.3. Sensitivity analysis

One goal of this research is the determination of support structure design parameters that have a large influence on the mechanical behaviour of the final part. The term mechanical behaviour stands partially in contrast to mechanical properties and includes the part's deformation and the formation of residual stresses during the build and after cool-down. It is in contrast to mechanical properties, since, for example, the density or tensile properties of the part are not taken into account. A sensitivity study is performed to determine the design parameters. The analysis uses the Advanced Meta-model of Optimal Prognosis (AMOP) approach from the optiSLang® plug-in for ANSYS® Workbench™ which is an extended version of the Meta-model of Optimal Prognosis (MOP) that was first introduced by Most and Will [36]. Polynomial regression can be used to approximate the response of a model. The Moving Least Squares (MLS) approximation [37] takes this one step further and introduces distance-dependent weighting functions for better approximation. These two prediction approaches build, together with the search for optimum input values, the base for the MOP [36]. The quality of the prediction can be checked using the Coefficient of Prognosis (CoP), which is a value calculated using the squared prediction errors and the total variation of the output. The result prediction is fast and computationally cheap compared to neural network approaches since no complex training algorithm is necessary for the AMOP. The meta-model is also suitable for additional parameter analysis or parameter optimisation and needs only a single solver run for verification [38].

In contrast to the more traditional full-factorial or fractional factorial Design of Experiments, the AMOP can keep the number of necessary solver runs to a minimum, while still keeping the prediction quality high. This is achieved by subsequently adding and solving design points until the CoP reaches a target value or the maximum number of desired design points is reached. The meta-model can be further refined by adding constraints for valid designs and optimisation objectives. One of these constraints is the sum of both parameters describing the straight part of the stem and the top branch, which needs to be smaller than 3 mm to keep a valid design. The second constraint that is introduced is to check the minimum distance of the stems, as the distance is driven by the seed point distance and the reduction factor. A third constraint is a failure criterion, which compares the maximum principal stress of the part with the ultimate tensile stress of the material following Rankine's theory for brittle materials.

Table 1 shows the lower and upper bounds of the support structure design parameters for the sensitivity analysis. The diameters of the tree-like structures were given a range of 0.5 mm to 0.8 mm based on tensile tests of a preceding study, which showed the best results for 0.6 mm and 0.7 mm [31]. The bounding values for the other parameters were determined by creating the support structure virtually until the resulting designs violated Design for Additive Manufacturing (DfAM) rules [26] or the trees were no longer identifiable as such.

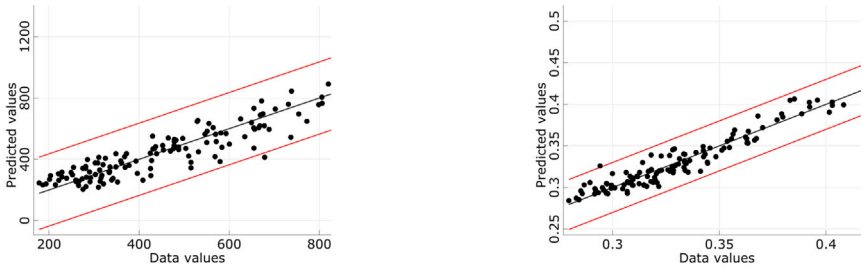

(a) Support volume response (b) Displacement response

Fig. 3. Residual plots: Predicted versus simulated values.

2.4. Parameter optimisation

Following the creation of the meta-model and the sensitivity analysis, parameter optimisation is performed. Therefore, an evolutionary algorithm is used, because of the relatively high number of input parameters and multiple objectives. These objectives are the minimisation of the support volume, i.e. respectively powder usage and build time, and the minimisation of the maximum nodal displacement after cool down, as this is a measure for the geometric accuracy of the part before heat treatment is performed. The maximum displacement is preferred over a stress objective because the displacement is better suited for an automated result evaluation as the stress shows sometimes peak values at singularities. Due to the fact, that the volume and the displacement objective are self-interfering, as low material usage – in general – contradicts support strength, a trade-off needs to be found. Therefore the admired result of the parameter optimisation is a Pareto frontier. A Pareto frontier is a set of Pareto optimal values, which are the result of a multi-objective optimisation, where improving one response would harm at least one other result value [39]. In this way, the designer can choose an optimal result between less material consumption or higher part deformation.

3. Results and discussion

In the following section, results of the performed simulations and the meta-model based optimisation are discussed. First, each geometry is handled individually, then subsequent comparisons of the results for Cantilever A and B are performed. The simulations were performed on a system with an Intel® Core™ i7-8700K processor and 32 GB RAM. A single simulation run took approximately 20 min, but parallelisation of up to five parameter sets was possible without a noticeable slow down.

3.1. Cantilever A

For Cantilever A, the AMOP is based on 500 samples, which was also the maximum allowed number of design points to be simulated. From these 500 DPs, 370 designs failed or were excluded from the meta-model generation due to unpredicted errors in the simulation model or because of constraint violations. Nevertheless, a CoP of 85% was achieved for the support volume response V_{tot} and a CoP of 94% for the displacement response Δ_{max}. These Coefficients of Prognosis are evaluated by the software and are close to the targeted 90% prognosis quality of the meta-model. For both responses, the input parameters k_{red} and l_{min} have the best prediction accuracy. The residual plots of these two input parameters are displayed with a confidence level of $\sigma = 3$ for the support volume response in Fig. 3(a) and the displacement response in Fig. 3(b).

The importance of the input parameters l_{min} and k_{red} is also reflected by their high correlation with the response V_{tot} with correlation values $r_{57} = -0.858$ and $r_{67} = -0.758$ as well as Δ_{max} with $r_{58} = 0.740$ and $r_{68} = 0.914$, see Fig. 4. Despite the also high correlations between the stem diameter and the responses ($r_{17} = 0.611$, $r_{18} = -0.685$), the top diameter shows no correlation with the responses at all. For this example, r_{17} means an increase of support volume, if the stem diameter is increased. For the negative sign of r_{18} this results in a reduction of the maximum displacement respectively. The self-interference of the responses described in Section 2.4 results in $r_{78} = -0.78$.

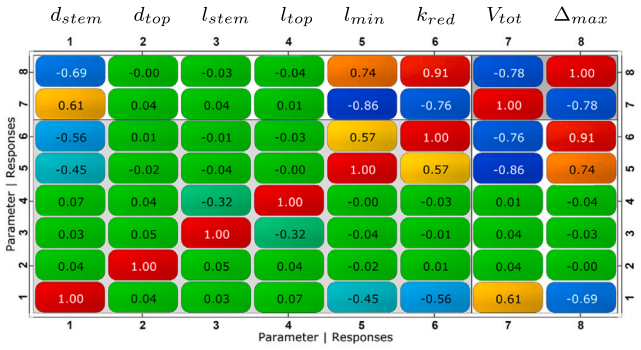

Fig. 4. Correlation matrix for parameters and responses of Cantilever A.

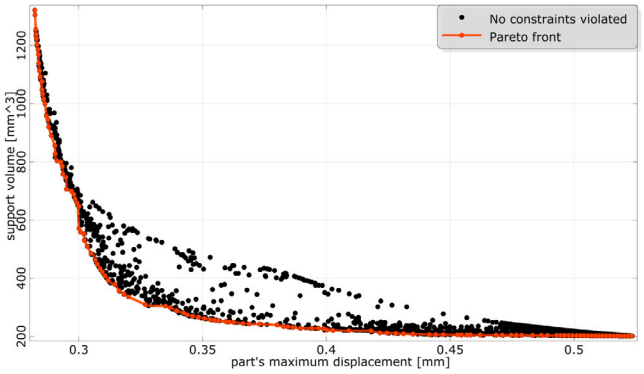

Fig. 5. Pareto plot for the objectives of Cantilever A.

Correlations of the input parameters to be mentioned are between l_{min} and d_{stem} with a negative correlation of $r_{15} = -0.454$ and for the stem reduction factor $r_{56} = 0.566$. The stem diameter shows an inverted behaviour to the stem reduction factor with $r_{16} = -0.565$. Further minor negative correlation can be seen for the input parameters l_{stem} and l_{top} with a value of $r_{34} = -0.321$. Other parameters show no noteworthy correlations. The full correlation matrix is displayed in Fig. 4.

The optimisation was performed with an evolutionary algorithm, evaluating 9000 samples using the meta-model. At least one of the previously defined constraints was violated for 553 of these samples. The objectives of the optimisation are the minimisation of both mentioned responses V_{tot} and Δ_{max}. As these responses, in general, contradict each other to some extent, no single optimum can be determined and the result is a Pareto plot, which is shown in Fig. 5.

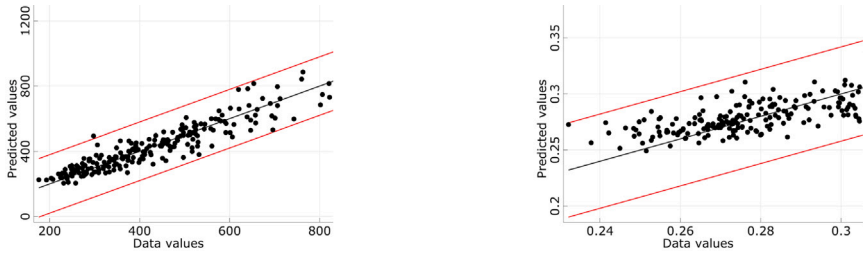

(a) Support volume response (b) Displacement response

Fig. 6. Residual plots: Predicted versus simulated values.

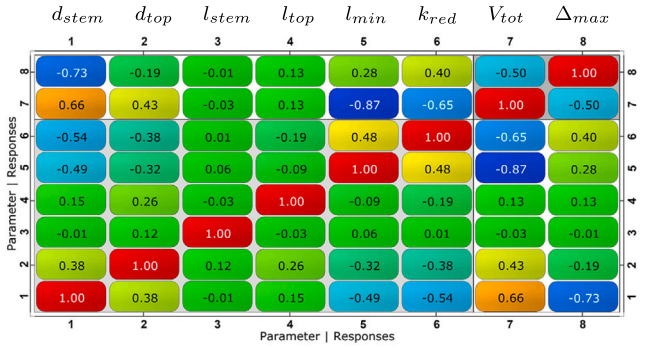

Fig. 7. Correlation matrix for parameters and responses of Cantilever B.

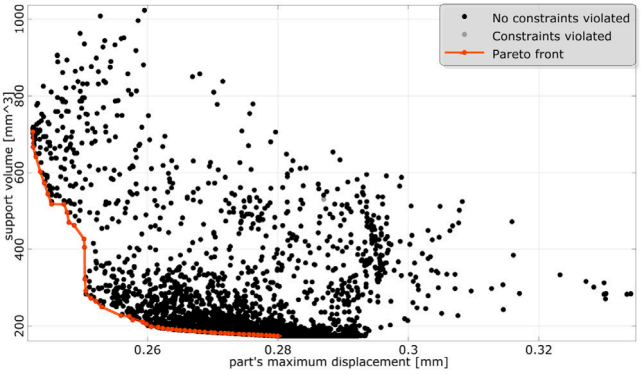

Fig. 8. Pareto plot for the objectives of Cantilever B.

The plot displays the values of both responses for each sample not violating any constraints as a point. The best designs are marked in orange and form the Pareto frontier. For Fig. 5, a distinctive Pareto frontier is visible with a recognisable asymptotic behaviour on both ends. For the displacement response, the asymptotic threshold value is located at approximately 0.28 mm, for the support volume, it is 200 mm^3. For a small region of interest, the input parameters leading to responses on the Pareto frontier are investigated and discussed in Section 3.3.

3.2. Cantilever B

For the second geometry, the meta-model was created using also 500 simulations with individual support structure design, from which 275 failed or were excluded due to simulation errors or constraint violations. Despite the larger amount of exploitable data points, the targeted 90% prognosis quality was not met. For the support volume response, a CoP of 87.5% was achieved, but the prognosis coefficient for the displacement response is substantially lower with a value of 59.6%. Following the results of geometry A, the best prediction accuracy was reached for the input parameters k_{red} and l_{stem}. The residual plots for both of them are displayed in Figs. 6(a) and 6(b) with a confidence level of $\sigma = 3$.

In contrast to the Cantilever A, the correlation between the stem reduction factor and the responses is lower with values of $r_{67} = 0.396$ and $r_{68} = -0.650$. Instead, the diameter of the stem shows high correlations with $r_{17} = 0.663$ for the volume response and $r_{18} = -0.731$ for the displacement response. The parameters d_{top} and l_{min} seem only to substantially affect the volume response with values of $r_{27} = 0.43$ and $r_{57} = -0.868$. The self-interference of the responses is with a value of $r_{78} = -0.502$ smaller than for the Cantilever A.

Correlations between the input parameters are similar to the ones from cantilever A, but there are more present. Values to be mentioned are the negative correlations between the stem diameter and the minimum distance with $r_{15} = -0.493$ as well as the reduction factor with $r_{16} = -0.544$. The top diameter shows less correlation with these two resulting in $r_{25} = -0.317$ and $r_{26} = -0.384$. Both diameters between each other are related with $r_{12} = 0.377$. Correlations between l_{min} and k_{red} are similar strong with a value of $r_{56} = 0.480$. Additionally, there is a minor correlation between the top diameter and the stem length with $r_{24} = 0.261$. Other correlations are not noteworthy. The full matrix is displayed in Fig. 7.

For Cantilever B, the optimisation of the two objectives V_{tot} and Δ_{max} meta-model was also performed with 9000 samples. In this case, only 138 of these sample points violated one or more of the constraints. The resulting Pareto plot is displayed in Fig. 8. A distinctive Pareto frontier can be seen and is marked in orange. Also, it is visible that the evolutionary algorithm led to a more dense section for lower support volume values. This might result in a slightly decreased accuracy of the Pareto frontier for large support volume values or small displacements respectively. The asymptotic behaviour of the frontier is less pronounced than for Cantilever A. For the support volume, the asymptotic threshold is around 180 mm^3. The displacement side on the other hand shows only a quasi asymptotic behaviour, which cannot be described with full certainty due to the mentioned inaccuracy. A threshold value for the maximum displacement can therefore only be assumed at 0.24 mm.

3.3. Comparison

The Coefficient of Prognosis for the displacement response of Cantilever B is substantially lower than the one for A. One possible reason for this is the more random distribution of result values for the input parameters k_{red} and l_{min}. Therefore a simple linear regression approximation as it is used for the Cantilever A is not sufficient and the more complex isotropic Kriging approximation is chosen by the software. The response surfaces are shown in Fig. 9(a) for Cantilever A and in 9(b) for Cantilever B respectively.

Comparing the correlation results for both geometries with each other, Cantilever A shows in general fewer correlations between input parameters than Cantilever B. Looking at the responses, it can be determined that correlations between input parameters and the

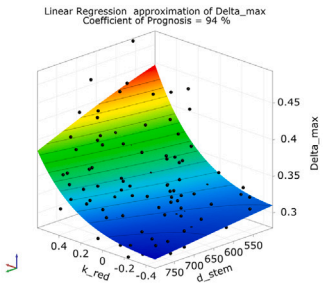

(a) Response surface Cantilever A

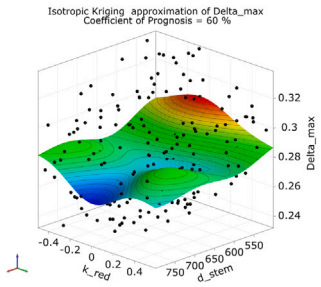

(b) Response surface Cantilever B

Fig. 9. Displacement response surfaces for Cantilever A and B.

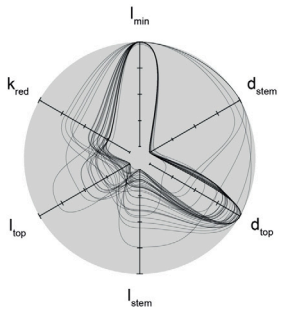

(a) Parameters of Cantilever A

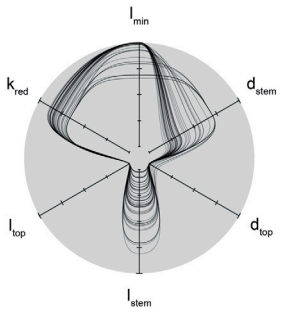

(b) Parameters of Cantilever B

Fig. 10. Parameter values in region of interest.

support volume have similar values, while the parameters l_{min} and k_{red} affect the displacement response of B significantly less than the one of Cantilever A. In addition, both the support volume and displacement values are lower at the Pareto frontier of Cantilever B than in A, which can be explained by the better printability of the arches in geometry B compared to the flat overhang in geometry A. To further compare the individual parameters, which lead to a result value on the Pareto frontier, a small region of interest was chosen for each geometry. For Cantilever A, this region ranges from 0.34 mm to 0.36 mm on the displacement axis and for Cantilever B from 0.25 mm to 0.27 mm as maximum displacement. Thereby a set of 40 samples is selected for A and a set of 59 samples for B. A spider-web plot, showing the parameter sets as splines, is displayed for each geometry in Figs. 10(a) and 10(b). It can be seen that for both geometries, the parameter l_{min} resolves in a Pareto design for values close to the upper bound and for l_{top}, values close to the lower bounds lead to better results. The latter might result from a better and more even heat conduction if the length of the branches is shorter. It can also be noticed that the parameters d_{top} and k_{red} seem to act in an inverse way depending on the geometry. While higher values of d_{top} are better for Cantilever A, B benefits from lower values. For the parameter k_{red}, this finding applies vice versa.

3.4. Physical implementation and verification

To verify the functionality of the optimised tree-support, the support structure was physically implemented for cantilever A and compared with commercially generated support. Block-support with perforation was generated using Materialise Magics' standard parameters, which resulted in a support volume of 246 mm^3. For the tree-like support, a Pareto optimal design was selected that matched the volume of the block-support. Both top and stem diameter were 0.8 mm with a minimum distance value of 1.5 mm between the branches. The stem reduction factor was 0.58 to ensure the low volume fraction of the block-support. As the removability of the support was not part of the investigation, the tree-like support was not altered in any way to facilitate support removal. Both parts were printed on the same build plate using Ti6Al4V powder on a Trumpf TruPrint 1000 PBF-LB/M machine. A layer height of 20 (mμ) was used with a laser power of 110 W at a scanning speed of 905 mm s^{-1} for the core strategy. The printed parts are shown in Fig. 11 in as-built condition.

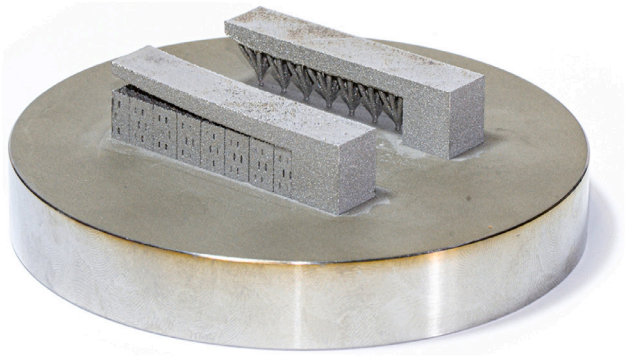

Fig. 11. PBF-LB/M printed cantilever in as-built condition with standard block-support and optimised tree-like support.

It can be observed that the block-support failed to fulfil its function in supporting the overhang region and anchoring the part to the base plate. The insufficient design of the support led to delamination at the support-part interface during the build, which resulted further in the residual stress-induced curling up of the overhanging region. The tree-like support on the other hand shows only minor warping of the unsupported free edge of the overhang surface, which has no effect on the geometric accuracy of the top surface. This can also be observed in Fig. 12, where the top surface displacement is displayed for measurements at the part's centre line in as-built condition and

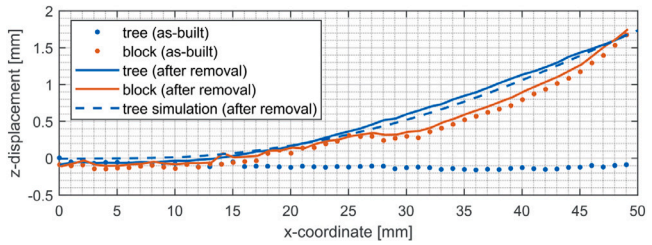

Fig. 12. Measured top surface displacement before (dotted) and after support removal with simulated displacement after removal (dashed).

after support removal. For both supports, the total deformation after support removal is almost identical, but the curve of the block-support sample increases at a steeper angle. In addition to the measurements on the printed parts, a FE simulation was performed for the selected tree-like support design. The resulting displacement values are within the dimensional accuracy of the measuring device and the error induced by the scaling factors of the simulation. Based on these results, the simulation model is considered to be verified. With the verified simulation model, also the optimisation is assumed to deliver reliable results for the Pareto frontier. The optimality of the individual results was not further investigated, as there is no single optimum for a Pareto optimisation, and the large number of necessary physical prints was considered uneconomically.

4. Conclusions

The study tackles the parameter optimisation of parameters in support structure design, utilising automatic support structure generation to quickly simulate multiple varying sample geometries for the optimisation. As supports, parametric tree-like structures are used. Two exemplary geometries in a cantilever design with different support faces are chosen, to determine, which parameters have similar behaviour. Nevertheless, the approach can be applied to any geometry. Additionally, standard block-support is outperformed by the Pareto optimised tree-like support with a matching support volume.

Results show that the stem diameter is an important parameter due to high correlations with the support volume response and the maximum displacement response of the part. Values in the lower third of the tested parameter range lead to the best designs. High correlations between input parameters and responses are also visible for the stem reduction factor and the minimum length between seed points, but only the second shows a similar behaviour between the two geometries with best results for parameter values at the upper boundary of the tested range. The stem reduction factor affects the results in an inverse manner between Cantilever A and B. Due to the self-interfering nature of both responses i.e. minimising the support volume increases the parts displacements, no single best design can be chosen and a Pareto frontier emerges from the results. Especially for the two different geometries, there is no set of support structure design parameters that leads in both cases to the best results. Comparing the results with a previous parameter investigation on support structure design [40], the high correlation between the stem diameter and the displacement is in accordance. This applies also to the correlation between the responses and the reduction factor combined with l_{min}, which are controlling the number of supports. Only the top diameter seems to be less important than assumed by the previous contribution.

Parameter optimisation has the potential to outperform topology optimisation for support structure generation in the optimisation speed. Once the meta-model is created, the optimisation can be performed in less than 10 min. Compared to neural network approaches, there is no need for a large set of training geometries. Future work could include similar studies for more geometries with differing support surfaces. In this way, meta-models for a set of surfaces that need support and commonly occur on parts can be created or design guidelines with results similar to Lammers et al. [41] can be derived. In addition, the removability of the supports could be addressed by adding additional design parameters for the tip design of the branches.

Declaration of competing interest

The authors declare that they have no known competing financial interests or personal relationships that could have appeared to influence the work reported in this paper.

Data availability

The raw data required to reproduce these findings cannot be shared due to legal reasons. The code for the automatic support generation cannot be shared at this time as it is part of an ongoing study.

Acknowledgements

The authors like to thank Bill Song and Christoph Petroll of the 3D Printing Center at the Bundeswehr Research Institute for Materials, Fuels and Lubricants (WIWeB) for the PBF-LB/M print of test samples in order to evaluate the strain scaling factors.

Funding

We acknowledge financial support by Universität der Bundeswehr München, Germany and the German Federal Ministry of Defense.

References

[1] Calignano F. Design optimization of supports for overhanging structures in aluminum and titanium alloys by selective laser melting. Mater Des 2014;64:203–13. http://dx.doi.org/10.1016/j.matdes.2014.07.043, URL https://linkinghub.elsevier.com/retrieve/pii/S0261306914005755.

[2] Diegel O, Nordin A, Motte D. A practical guide to design for additive manufacturing. Springer Series in Advanced Manufacturing, Springer Singapore; 2019, http://dx.doi.org/10.1007/978-981-13-8281-9, URL https://www.springer.com/de/book/9789811382802.

[3] Wiberg A, Persson J, Ölvander J. Design for additive manufacturing – a review of available design methods and software. Rapid Prototyp J 2019;25(6):1080–94. http://dx.doi.org/10.1108/RPJ-10-2018-0262, URL https://www.emerald.com/insight/content/doi/10.1108/RPJ-10-2018-0262/full/html.

[4] Gaynor AT, Guest JK. Topology optimization considering overhang constraints: Eliminating sacrificial support material in additive manufacturing through design. Struct Multidiscip Optim 2016;54(5):1157–72. http://dx.doi.org/10.1007/s00158-016-1551-x, URL http://link.springer.com/10.1007/s00158-016-1551-x.

[5] Garaigordobil A, Ansola R, Veguería E, Fernandez I. Overhang constraint for topology optimization of self-supported compliant mechanisms considering additive manufacturing. Comput Aided Des 2019;109:33–48. http://dx.doi.org/10.1016/j.cad.2018.12.006, URL https://linkinghub.elsevier.com/retrieve/pii/S001044851830349X.

[6] Xu S, Liu J, Ma Y. Residual stress constrained self-support topology optimization for metal additive manufacturing. Comput Methods Appl Mech Engrg 2022;389:114380. http://dx.doi.org/10.1016/j.cma.2021.114380, URL https://linkinghub.elsevier.com/retrieve/pii/S0045782521006423.

[7] Höller C, Zopf P, Schwemberger P, Pichler R, Haas F. Load capacity of support structures for direct machining of selective laser melted parts. In: Volume 2A: Advanced manufacturing. Salt Lake City, Utah, USA: American Society of Mechanical Engineers; 2019, http://dx.doi.org/10.1115/IMECE2019-11134, URL https://asmedigitalcollection.asme.org/IMECE/proceedings/IMECE2019/59377/Salt%20Lake%20City,%20Utah,%20USA/1072798.

[8] Didier P, Le Coz G, Robin G, Lohmuller P, Piotrowski B, Moufki A, Laheurte P. Consideration of SLM additive manufacturing supports on the stability of flexible structures in finish milling. J Manuf Process 2021;62:213–20. http://dx.doi.org/10.1016/j.jmapro.2020.12.027, URL https://linkinghub.elsevier.com/retrieve/pii/S152661252030863X.

[9] Patterson AE, Messimer SL, Farrington PA. Overhanging features and the SLM/DMLS residual stresses problem: Review and future research need. Technologies 2017;5(2):15. http://dx.doi.org/10.3390/technologies5020015, URL https://www.mdpi.com/2227-7080/5/2/15.

[10] Cheng L, Liang X, Bai J, Chen Q, Lemon J, To A. On utilizing topology optimization to design support structure to prevent residual stress induced build failure in laser powder bed metal additive manufacturing. Addit Manuf 2019;27:290–304. http://dx.doi.org/10.1016/j.addma.2019.03.001, URL https://linkinghub.elsevier.com/retrieve/pii/S2214860418309035.

[11] Hussein A, Hao L, Yan C, Everson R, Young P. Advanced lattice support structures for metal additive manufacturing. J Mater Process Technol 2013;213(7):1019–26. http://dx.doi.org/10.1016/j.jmatprotec.2013.01.020, URL http://www.sciencedirect.com/science/article/pii/S092401361300037X.

[12] Subedi SC, Verma CS, Suresh K. A review of methods for the geometric post-processing of topology optimized models. J Comput Inf Sci Eng 2020;20(6):060801. http://dx.doi.org/10.1115/1.4047429, URL https://asmedigitalcollection.asme.org/computingengineering/article/doi/10.1115/1.4047429/1084391/A-Review-of-Methods-for-the-Geometric.

[13] Mezzadri F, Bouriakov V, Qian X. Topology optimization of self-supporting support structures for additive manufacturing. Addit Manuf 2018;21:666–82. http://dx.doi.org/10.1016/j.addma.2018.04.016, URL https://linkinghub.elsevier.com/retrieve/pii/S2214860418301519.

[14] Zhang Z, Ibhadode O, Ali U, Dibia C, Rahnama P, Bonakdar A, Toyserkani E. Topology optimization parallel-computing framework based on the inherent strain method for support structure design in laser powder-bed fusion additive manufacturing. Int J Mech Mater Design 2020. http://dx.doi.org/10.1007/s10999-020-09494-x.

[15] Liu Y, Li Z, Wei P, Chen S. Generating support structures for additive manufacturing with continuum topology optimization methods. Rapid Prototyp J 2019;25(2):232–46. http://dx.doi.org/10.1108/RPJ-10-2017-0213, URL https://www.emerald.com/insight/content/doi/10.1108/RPJ-10-2017-0213/full/html.

[16] Malekipour E, Tovar A, El-Mounayri H. Heat conduction and geometry topology optimization of support structure in laser-based additive manufacturing. In: Wang J, Antoun B, Brown E, Chen W, Chasiotis I, Huskins-Retzlaff E, Kramer S, Thakre PR, editors. Mechanics of additive and advanced manufacturing. vol. 9, Cham: Springer International Publishing; 2018, p. 17–27. http://dx.doi.org/10.1007/978-3-319-62834-9_4, URL http://link.springer.com/10.1007/978-3-319-62834-9_4.

[17] Zhou M, Liu Y, Lin Z. Topology optimization of thermal conductive support structures for laser additive manufacturing. Comput Methods Appl Mech Engrg 2019;353:24–43. http://dx.doi.org/10.1016/j.cma.2019.03.054, URL https://linkinghub.elsevier.com/retrieve/pii/S0045782519301938.

[18] Miki T, Nishiwaki S. Topology optimization of the support structure for heat dissipation in additive manufacturing. Finite Elem Anal Des 2022;203:103708. http://dx.doi.org/10.1016/j.finel.2021.103708, URL https://linkinghub.elsevier.com/retrieve/pii/S0168874X21001803.

[19] Subedi SC, Thoma DJ, Suresh K. Truss-type support structures for SLM. Publisher: University of Texas at Austin; 2021, http://dx.doi.org/10.26153/TSW/17635, URL https://repositories.lib.utexas.edu/handle/2152/90716.

[20] Allaire G, Bogosel B. Optimizing supports for additive manufacturing. Struct Multidiscip Optim 2018;58(6):2493–515. http://dx.doi.org/10.1007/s00158-018-2125-x, URL http://link.springer.com/10.1007/s00158-018-2125-x.

[21] Giraldo-Londoño O, Mirabella L, Dalloro L, Paulino GH. Multi-material thermomechanical topology optimization with applications to additive manufacturing: Design of main composite part and its support structure. Comput Methods Appl Mech Engrg 2020;363. http://dx.doi.org/10.1016/j.cma.2019.112812, URL https://linkinghub.elsevier.com/retrieve/pii/S0045782519307042.

[22] Zhang Y, Wang Z, Zhang Y, Gomes S, Bernard A. Bio-inspired generative design for support structure generation and optimization in additive manufacturing (AM). CIRP Annals 2020;69(1):117–20. http://dx.doi.org/10.1016/j.cirp.2020.04.091, URL http://www.sciencedirect.com/science/article/pii/S000785062030113X.

[23] Prusinkiewicz P, Lindenmayer A. The algorithmic beauty of plants. Springer Science & Business Media; 2012.

[24] Prusinkiewicz P. Applications of L-systems to computer imagery. In: Goos G, Hartmanis J, Barstow D, Brauer W, Brinch Hansen P, Gries D, Luckham D, Moler C, Pnueli A, Seegmüller G, Stoer J, Wirth N, Ehrig H, Nagl M, Rozenberg G, Rosenfeld A, editors. Graph-grammars and their application to computer science. Lecture Notes in Computer Science, vol. 291, Berlin, Heidelberg: Springer Berlin Heidelberg; 1987, p. 534–48. http://dx.doi.org/10.1007/3-540-18771-5_74, URL http://link.springer.com/10.1007/3-540-18771-5_74.

[25] Sun R, Jia J, Jaeger M. Intelligent tree modeling based on L-system. In: 2009 IEEE 10th international conference on computer-aided industrial design conceptual design. 2009, p. 1096–100. http://dx.doi.org/10.1109/CAIDCD.2009.5375256.

[26] Thomas D. The development of design rules for selective laser melting (Ph.D. thesis), Wales: University of Wales; 2009, URL https://repository.cardiffmet.ac.uk/handle/10369/913, Accepted: 2010-05-24.

[27] Wang D, Yang Y, Yi Z, Su X. Research on the fabricating quality optimization of the overhanging surface in SLM process. Int J Adv Manuf Technol 2013;65(9–12):1471–84, Publisher: Springer.

[28] Wang Z, Zhang Y, Tan S, Ding L, Bernard A. Support point determination for support structure design in additive manufacturing. Addit Manuf 2021;47:102341. http://dx.doi.org/10.1016/j.addma.2021.102341, URL https://linkinghub.elsevier.com/retrieve/pii/S2214860421004991.

[29] Mayer T, Brändle G, Schönenberger A, Eberlein R. Simulation and validation of residual deformations in additive manufacturing of metal parts. Heliyon 2020;6(5):e03987. http://dx.doi.org/10.1016/j.heliyon.2020.e03987, URL http://www.sciencedirect.com/science/article/pii/S240584402030832X.

[30] Krol TA, Zaeh MF, Seidel C. Optimization of supports in metal-based additive manufacturing by means of finite element models. In: SFF symposium preceedings. Austin, TX, USA; 2012, p. 707–18.

[31] Weber S, Montero J, Petroll C, Schäfer T, Bleckmann M, Paetzold K. The fracture behavior and mechanical properties of a support structure for additive manufacturing of ti-6al-4V. Crystals 2020;10(5):343. http://dx.doi.org/10.3390/cryst10050343, URL https://www.mdpi.com/2073-4352/10/5/343.

[32] Weber S, Montero J, Bleckmann M, Paetzold K. A comparison of layered tetrahedral and cartesian meshing in additive manufacturing simulation. In: Enhancing design through the 4th Industrial Revolution Thinking, Procedia CIRP In: Enhancing design through the 4th Industrial Revolution Thinking, 2020;91:522–7. http://dx.doi.org/10.1016/j.procir.2020.02.209.URL http://www.sciencedirect.com/science/article/pii/S221282712030860X,

[33] Li C, Gouge MF, Denlinger ER, Irwin JE, Michaleris P. Estimation of part-to-powder heat losses as surface convection in laser powder bed fusion. Addit Manuf 2019;26:258–69. http://dx.doi.org/10.1016/j.addma.2019.02.006, URL https://linkinghub.elsevier.com/retrieve/pii/S2214860418306535.

[34] Stephan P, Kabelac S, Kind M, Mewes D, Schaber K, Wetzel T, editors. VDI-wärmeatlas : Fachlicher träger VDI-gesellschaft verfahrenstechnik und chemieingenieurwesen, 12. VDI Springer Reference, Springer Vieweg; 2019, http://dx.doi.org/10.1007/978-3-662-52989-8, URL https://www.springer.com/de/book/9783662529881.

[35] Romano J, Ladani L, Sadowski M. Thermal modeling of laser based additive manufacturing processes within common materials. Procedia Manufact 2015;1:238–50. http://dx.doi.org/10.1016/j.promfg.2015.09.012, URL https://linkinghub.elsevier.com/retrieve/pii/S2351978915010124.

[36] Most T, Will J. Meta-model of optimal prognosis - an automatic approach for variable reduction and optimal meta-model selection. In: Proceedings of Weimar optimization and stochastic days 2008. 5, Weimar; 2008, p. 22.

[37] Lancaster P, Salkauskas K. Surfaces generated by moving least squares methods. Math Comp 1981;1(37):141–58. http://dx.doi.org/10.1090/S0025-5718-1981-0616367-1.

[38] Most T, Will J. Metamodel of optimal prognosis. In: Proceedings of Weimar optimization and stochastic days 2011. 8, Weimar; 2011, p. 17.

[39] Costa NR, Lourenço JA. Exploring Pareto frontiers in the response surface methodology. In: Yang G-C, Ao S-I, Gelman L, editors. Transactions on engineering technologies. Dordrecht: Springer Netherlands; 2015, p. 399–412. http://dx.doi.org/10.1007/978-94-017-9804-4_27.

[40] Weber S, Montero J, Bleckmann M, Paetzold K. Parameters on support structure design for metal additive manufacturing. Proc Design Soc: Des Conf 2020;1:1145–54. http://dx.doi.org/10.1017/dsd.2020.14, URL https://www.cambridge.org/core/product/identifier/S263377622000014X/type/journal_article.

[41] Lammers S, Lieneke T, Zimmer D. Development of a method to derive design guidelines for production-suitable support structures in metal laser powder bed fusion. Publisher: University of Texas at Austin; 2021, http://dx.doi.org/10.26153/TSW/17550, URL https://repositories.lib.utexas.edu/handle/2152/90631.